PHYSICAL REVIEW B **93**, 144102 (2016)

Asymmetric structure of 90° domain walls and interactions with defects in $PbTiO_3$

Anand Chandrasekaran,[1,2] Xian-Kui Wei,[2,3] Ludwig Feigl,[2,4] Dragan Damjanovic,[2] Nava Setter,[2] and Nicola Marzari[1,5]

[1]*Theory and Simulation of Materials, École Polytechnique Fédérale de Lausanne (EPFL), 1015 Lausanne, Switzerland*

[2]*Ceramics Laboratory, École Polytechnique Fédérale de Lausanne (EPFL), 1015 Lausanne, Switzerland*

[3]*Peter Grünberg Institute and Ernst Ruska Center for Microscopy and Spectroscopy with Electrons, Research Center Jülich, D-52425 Jülich, Germany*

[4]*Institute for Photon Science and Synchrotron Radiation, KIT - Karlsruhe Institute of Technology, Hermann-von-Helmholtz-Platz 1, D-76344 Eggenstein-Leopoldshafen, Germany*

[5]*National Centre for Computational Design and Discovery of Novel Materials (MARVEL), École Polytechnique Fédérale de Lausanne (EPFL), 1015 Lausanne, Switzerland*

(Received 8 March 2016; published 4 April 2016)

We investigate the atomistic structure of ferroelastic-ferroelectric 90° domain walls in $PbTiO_3$ with first-principles calculations and high-resolution scanning transmission electron microscopy. We find sharp discontinuities in the variation of lattice parameters across the domain walls. Unexpectedly, the two neighboring domains become asymmetric across the boundary, giving rise to primitive unit cells with large tetragonality ratios (c/a) of the order of 1.11 close to the boundary. The variation of the domain wall structure with respect to strain is demonstrated. We show that oxygen vacancies are attracted to the plane adjacent to the 90° domain wall. The mechanisms of domain wall pinning by oxygen vacancies is explained based on the energy landscape of the vacancies in the presence of the domain interface.

DOI: 10.1103/PhysRevB.93.144102

I. INTRODUCTION

Multiferroic oxides are materials of great technological interest and exhibit a variety of phenomena that are being investigated from a fundamental or applied perspective. Ferroelectric oxides especially have been long studied because of their excellent piezoelectric and dielectric properties. A new direction that raises much interest in these materials is related to the newly discovered properties of domain wall interfaces. For example, the presence of switchable polarization within a 180° domain wall of $PbTiO_3$ was reported recently by Wojdeł and Íñiguez [1]. Strongly charged domain walls have been discovered which show the presence of quantum two-dimensional electron gas [2,3] reminiscent of the phenomena observed in $LaAlO_3$/SrTiO heterostructures [4–6]. Charge separation in such domain walls has been exploited not only in oxides [7], but also in organometallic perovskites; it is thought that domain wall engineering is a promising approach to optimize photovoltaic devices [8]. More and more effort is being devoted to achieve the controlled growth and functionalization of such domain wall interfaces, especially in thin films [9–11].

The interaction of oxygen vacancies with domain walls has long been thought to influence the properties of ferroelectric materials. For example, the orientation of metal-oxygen vacancy defect associates causes the "aging" phenomena in doped ferroelectric ceramics [12–14] and single crystals [15]. The accumulation of oxygen vacancies is believed to be one of the causes behind the phenomenon of ferroelectric fatigue [16,17]. More recently, Sluka *et al.* [2] suggested that oxygen vacancies accumulate at tail-to-tail charged domain walls in $BaTiO_3$. Becher *et al.* [18] showed how coupling of oxygen vacancies with domain walls in $SrMnO_3$ altered the conductive properties of the wall with respect to the bulk. Chandrasekaran *et al.* [19] highlighted the attraction of oxygen vacancies and defect associates to 180° domain walls in $PbTiO_3$. Kitanaka *et al.* [20] reported the attractive potential of oxygen vacancies to 90° domain walls in $PbTiO_3$ using first-principles calculations and attributed this result partially to the electrostatic interaction of domain walls with the defect. Very recently, Xu *et al.* [21] suggest that the presence of oxygen vacancies at domain walls may lead to a magnetism due to a localized spin moment at the vacancy.

In this paper we first report observations on the structure of 90° domain walls in $PbTiO_3$. An asymmetry in the variation of the lattice parameter across the domain wall is shown both computationally and by high-resolution scanning transmission-electron-microscopy (HRSTEM) measurements. The variation of the structural asymmetry in the presence of strain is studied. We then investigate the interaction of such walls with different types of oxygen vacancies. The possible pinning mechanisms involving oxygen vacancies are studied, and it is suggested that the interaction of oxygen vacancies with domain walls arises mainly from elastic interactions as opposed to electrostatic ones.

II. COMPUTATIONAL DETAILS

We used density functional theory with the PBEsol XC approximation using ultrasoft pseudopotentials[1] and plane waves, as implemented in the QUANTUM ESPRESSO distribution [22]. An effective Monkhorst-Pack k-point mesh of $8 \times 8 \times 8$ per five-atom cell, a plane-wave cutoff of 60 Ry, and a charge density cutoff of 600 Ry are utilized. The plane-wave cutoff is chosen to converge the forces on atoms to 10^{-4} Ry/bohr. Since the supercells contain charged defects, a compensating jellium background of opposite charge is inserted to remove divergencies. The size of the supercell for the 90° domain wall calculation is $17.55a \times a \times 1.46a$,

[1]Pb.pbesol-dn-rrkjus_psl.0.2.2.UPF, Ti.pbesol-spn-rrkjus_psl.0.2.3.UPF, O.pbesol-n-rrkjus_psl.0.1.UPF

where a is the calculated lattice parameter of $PbTiO_3$ (3.87 Å). The construction of the supercell is performed in a similar manner to that of Meyer and Vanderbilt [23]. For calculations involving defects, the supercell size was $8.77a \times 2a \times 2.93a$. The supercell is thus doubled in the y and z directions to avoid strong interaction of vacancies with their periodic images and to reduce the effective planar concentration of vacancies in the y-z plane.

III. EXPERIMENTAL DETAILS

Lead zirconate titanate (PZT) 10/90 (10% zirconium and 90% titanium) thin films were prepared for experimental verification. The details of the sample preparation are given elsewhere [9]. The films are 160 nm thick and are sufficiently thick to minimize substrate effects. The cross-sectional PZT 10/90 specimens used for electron microscopy observation were prepared by conventional methods, including grinding, dimpling, polishing, and milling by argon ions. The atom-resolved high-angle annular-dark-field (HAADF) experiments were performed on a probe-corrected FEI Titan 80-200 microscope, operated at 200 kV. A two-dimensional Gaussian profile fitting to each individual Pb column was used to determine the lattice parameters from the HAADF-STEM image.

IV. RESULTS

The domain wall region of the relaxed supercell is shown in the schematic of Fig. 1. We look at the lattice parameter variation across the supercell by measuring the Pb-to-Pb distance along a particular direction. Hence, moving across the domain wall, we expect a smooth inversion of the a-c lattice parameters [24] due to the 90° rotation at the wall. However, from Fig. 2(a) it is seen that this variation is not smooth at all and it is not symmetric with respect to the plane of the domain wall. We define the "tail" part as the side of the domain wall in which the polarization vector is pointing away from the wall. The "head" refers to the part in which the polarization is pointing into the domain wall. We observe

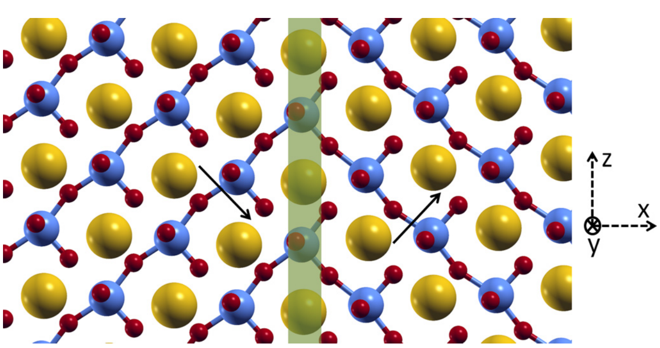

FIG. 1. Schematic showing the relaxed supercell of the 90° domain wall. The large yellow spheres are lead atoms, blue sphere are titanium, and small red spheres are oxygen. The domain wall plane is represented by the vertical green region across the middle of the figure. Black arrows in the figure show the direction of polarization in each domain. The x, y, and z directions are represented by the dashed lines on the right.

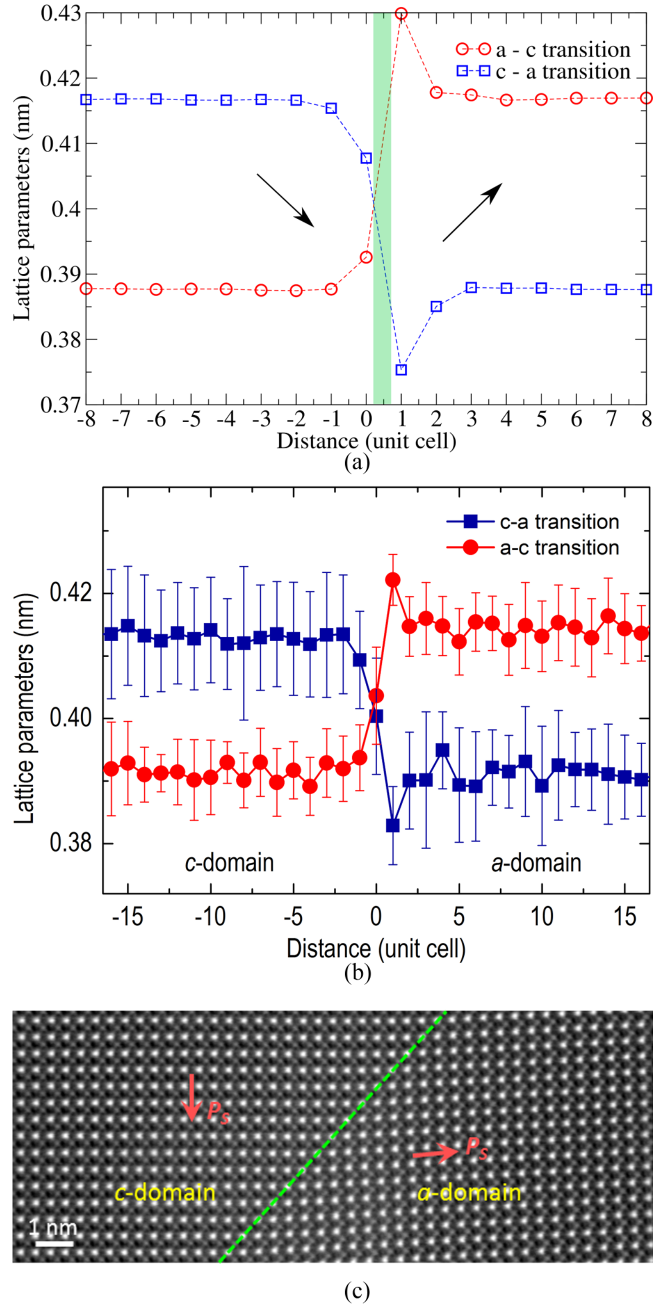

FIG. 2. (a) Variation of the lattice parameter across the domain wall as found in first-principles calculation on $PbTiO_3$. The shaded green region represents the approximate region of the domain wall plane, and the black arrows show the general direction of polarization in each domain. (b) Experimental measurements on PZT 10/90 thin film. (c) Atom-resolved HAADF-STEM image of a,c domain and domain wall viewed along [010] direction in 160-nm-thick PZT 10/90 thin film. The red arrows indicate direction of spontaneous polarization.

a large discontinuity of the lattice parameter variation at the domain walls; specifically, at the "tail" part of the domain wall there is a sharp dip in the a-c transition and a sharp peak in the c-a transition. This leads to a unit cell with large c/a ratio of 1.11 on the tail side of the domain wall. In comparison, the left side of the domain wall (i.e., the "head" part) shows a very smooth variation of the lattice parameters. Calculations were also performed for longer supercells (up to 240 atoms) and shorter supercells (60 atoms) to verify that this discontinuity is independent of supercell length.

Probe-corrected scanning transmission electron microscopy (STEM) was used to identify this asymmetry experimentally. Figure 2(b) shows the lattice parameter variation across the domain wall measured in PZT 10/90 (10% zirconium and 90% titanium). This material is tetragonal, having very close lattice parameters to those of the calculated $PbTiO_3$, as evident by the y axis on both Figs. 2(a) and 2(b). Comparing with first-principles results, we see a quantitative and qualitative agreement in the *a*-*c* transition (red circles) and the *c*-*a* transition (blue squares). The c/a ratio of the unit cell (both experimental and first principles) is presented in Fig. 3. We see that the domain wall is 4–5 unit cells wide, as predicted in our calculations.

These highly accurate measurements verify the presence of this asymmetry in the 90° domain wall structure. Stemmer *et al.* [24] were the first to observe the structure of the 90° domain wall in $PbTiO_3$ using conventional high-resolution transmission electron microscopy. However, the accuracy of such measurements were much lower, and they predicted a continuous symmetric lattice parameter variation. On closer inspection of their data points we see hints of this discontinuity which were verified by our highly accurate STEM measurements.

Although this observation seems surprising at first, reasons for it become clearer when considering the inherent asymmetric nature of most ferroelectric interfaces and surfaces. Consider a ferroelectric thin film with polarization pointing out of the plane of the film. This positively charged surface will show the presence of ionic reconstructions to minimize the bound polarization charge on the surface. Once the polarization is reversed, the surface will restructure in a completely different way. This was best illustrated in the recent work by Saidi *et al.* [25] on the interaction of polarization with surface stoichiometry in $PbTiO_3$ and $BaTiO_3$. Indeed, Meyer and Vanderbilt [23] reported the presence of an electrostatic potential at 90° domain walls in $PbTiO_3$ due to the breaking of mirror symmetry across the wall. Zhang and Goddard [26] obtained a similar asymmetric structure of the 90° domain wall in $BaTiO_3$ using first-principles-based model potentials. However, they report a much larger size of the domain wall in $BaTiO_3$ compared to what is observed by us in $PbTiO_3$.

It was of interest to see the effect of strain on this asymmetry in the 90° domain wall. The supercell was strained in the x, y, and z directions (for axis refer to Fig. 1). The domain wall structure was not very sensitive to low strain deformations. However, as depicted in Fig. 4, we see drastic changes in the lattice parameter variations across the domain wall in the presence of larger strains of 2%. We see especially that the c/a ratio on the tail side of the wall is quite sensitive to strains in the z direction. Specifically, tensile strain on the z direction leads to a larger c/a ratio on the tail side of the wall, while compressive strain of 2% in the z direction leads to a symmetric and smooth variation of the lattice parameter across the domain wall.

Next, we sought to understand the interaction of these domain walls with oxygen vacancies. Hybrid density-functional-theory calculations on $PbTiO_3$ have established the oxygen vacancy as being doubly positively charged [27] in such

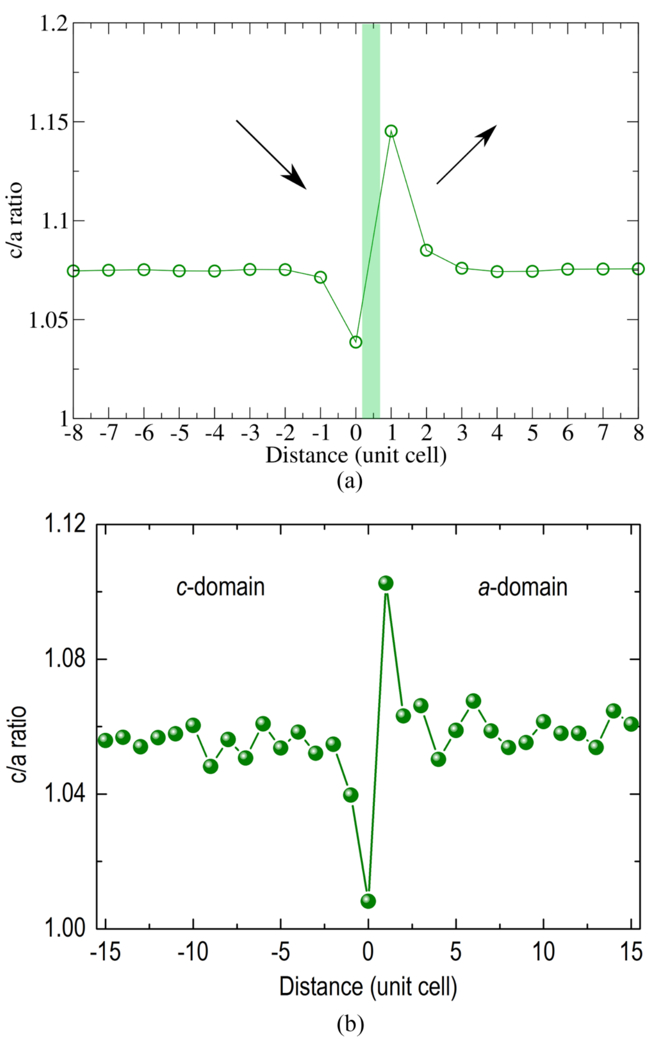

FIG. 3. Variation of the c/a ratio across the domain wall as found in (a) first-principles calculation on $PbTiO_3$ and (b) experimental measurements on PZT 10/90 thin film.

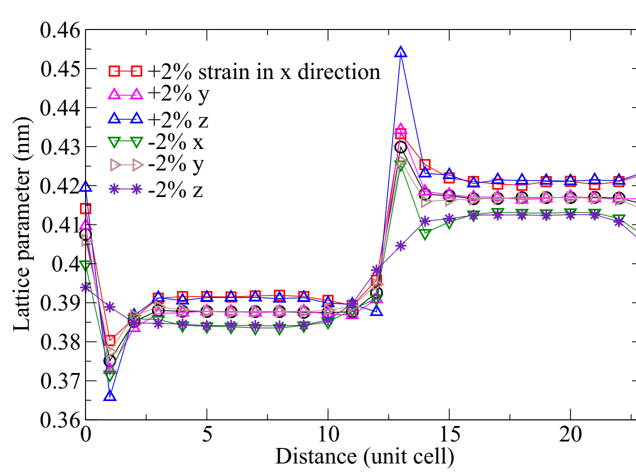

FIG. 4. Variation of lattice parameter across the domain wall with 2% lattice strains in different directions. The domain structure is especially sensitive to strains in the z direction.

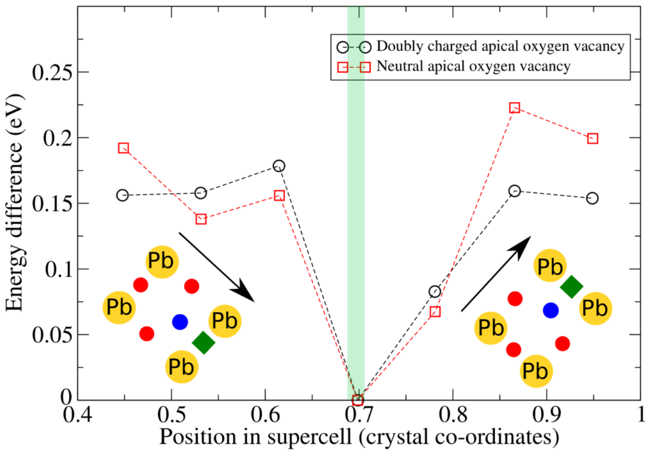

(a)

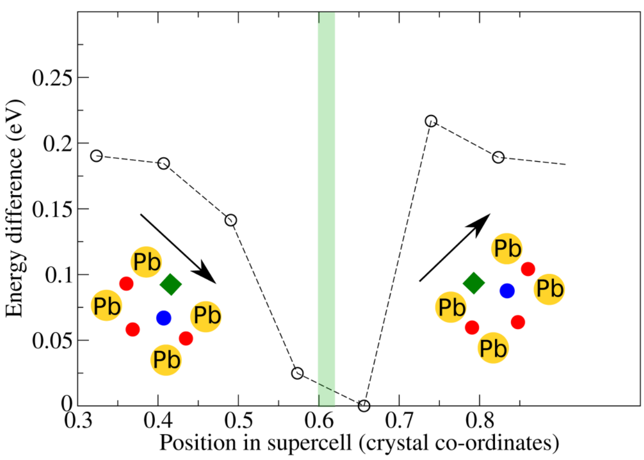

(b)

FIG. 5. (a) Stability of charged and neutral apical oxygen vacancy at different positions along the supercell. Yellow circles are lead, red circles are oxygen, blue circle is titanium, and green square represents an oxygen vacancy. The energies are plotted with respect to the lowest energy positions in the supercell. (b) Stability of charged equatorial oxygen vacancy at different positions along the supercell.

ferroelectric oxides. In this work we mainly look at the interaction of charged oxygen vacancies with the 90° domain walls studied above. Due to the tetragonal symmetry of $PbTiO_3$, there are two types of oxygen vacancies: apical (V_{ap}) and equatorial (V_{eq}). The apical vacancies, located on the apex of the oxygen octahedra, are known to be energetically more favorable compared to the equatorial vacancies [27–29] (located in the equatorial plane of the octahedra). In our calculations, we calculate the energy difference between the apical and equatorial position to be 0.40 eV in the bulk.

First, we looked at the stability of both charged and neutral apical oxygen vacancies at different positions with respect to the domain wall. The energy landscape is plotted in Fig. 5(a), and the most stable position of both the charged and neutral apical oxygen vacancy is depicted in Fig. 6. The ground-state oxygen vacancy position is not located exactly on the plane of the domain wall but is in fact located on the adjacent plane (on the "tail" side of the domain wall). It has been postulated that oxygen vacancies can stabilize strongly charged tail-to-tail

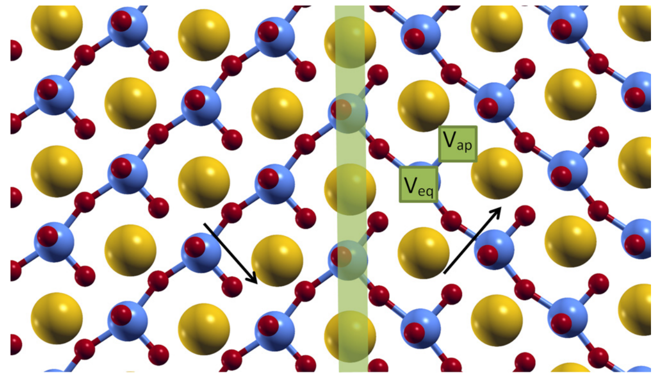

FIG. 6. Schematic showing the ground-state positions of the apical oxygen vacancy (V_{ap}) and equatorial oxygen vacancy (V_{eq}). The large yellow spheres are lead atoms, blue sphere are titanium, small red spheres are oxygen. The domain wall plane is represented by the vertical green region across the middle of the figure. Black arrows in the figure show the direction of polarization in each domain.

domain walls [3]. Indeed, from our calculations we observe that apical oxygen vacancies are more stable on the tail side of the domain rather than the head side. These results are in agreement with that of Kitanaka *et al.* [20] and Xu *et al.* [21]. Another important point to observe is that both charged and neutral oxygen vacancies exhibit similar interaction with the 90° domain wall. This indicates that the attraction of oxygen vacancies to domain walls is predominantly an elastic interaction rather than an electrostatic interaction. Therefore it is very likely that the large c/a ratio on the tail side of the wall stabilizes the oxygen vacancy. Recent work by Becher *et al.* [18] has shown that the formation energy of oxygen vacancies does indeed depend on the strain. The relative stability of equatorial oxygen vacancies is shown in Fig. 5(b). The equatorial oxygen vacancy is also preferably positioned on the tail side but it does not show as strong a specificity as the apical oxygen. This is likely due to the fact that equatorial vacancies do not interact with polarization as strongly as apical oxygen vacancies [27]. Apical vacancies are even thought to invert the polarization locally [16,17] due to this strong interaction.

Note that the ground-state equatorial oxygen vacancy would prefer to migrate to the apical oxygen vacancy ground-state position since the energy difference between these two is calculated by us to be 0.44 eV. As mentioned before, this energy difference is due to the nondegenerate nature of apical and equatorial oxygen vacancies in tetragonal oxides. The movement of the 90° domain wall requires short-range displacement of atoms, while the movement of oxygen vacancies requires the migration of oxygen atoms. The two processes have vastly different energy scales. The barrier energy for the movement of 90° domain wall in the absence of defects [30] is less than 1 mJ/m^2 (of the order of few millielectronvolts per unit cell), while oxygen vacancies have migration activation energies of up to 0.9 eV [19]. Hence, at low temperatures, the defects are unlikely to move (or they move slowly) with respect to the domain wall. Consider a situation in which an *apical* oxygen vacancy exists in one domain a few nanometers from a 90° domain wall. The movement of a domain wall

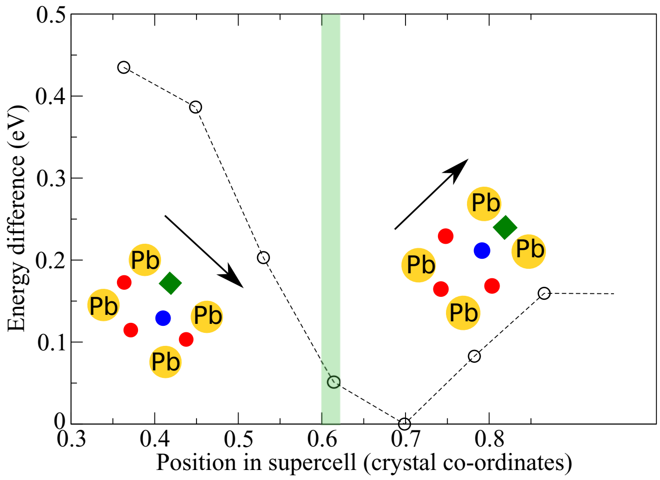

FIG. 7. Graph illustrating the pinning of 90° domain walls by oxygen vacancies. On the right side of the figure the oxygen vacancy is in the low-energy apical state. Close to the domain wall, on the tail side (crystal coordinates 0.7), it is in its ground-state position. If the domain wall continues to move, the vacancy transforms to the high-energy equatorial state depicted on the left side of the figure.

across the defect will cause it to transform into an energetically unfavorable *equatorial* vacancy. Hence it will oppose the motion of the domain wall towards its direction. We can capture this situation using first-principles calculations as depicted in Fig. 7. On the right side of the figure the oxygen vacancy is in the low-energy apical state. Close to the domain wall it is in its ground-state position. If the domain wall continues to move, the vacancy transforms to the high-energy equatorial state depicted on the left side of the figure. It prefers to exist in certain domain orientations compared to others, but it also prefers to exist close to the domain wall. In other terms, the oxygen vacancy behaves both as a "random-bond" [30–32] defect and "random-field" [14,33] defect. A random-field defect has an asymmetric effect on the ferroelectric electric double well, while the random-bond defect produces a symmetric modification of the double well. Based on Fig. 7, we may say there are two pinning regimes. We start at low temperatures where we define oxygen vacancies to be randomly distributed, thus behaving purely as random-field defects. At higher temperatures and longer time scales, oxygen vacancies would aggregate close to the domain wall (the global minimum) and would then also possess random-bond components, since it would pin the domain wall from movement in either direction of the interface. Such an existence of two regimes of pinning was also demonstrated in the experimental work of Morozov and Damjanovic on PZT [34].

V. CONCLUSION

In conclusion, we observe a strong structural asymmetry in 90° domain walls in $PbTiO_3$ highlighting the presence of a plane of large tetragonality on the tail side of the domain wall. These results contradict earlier experimental observations that pointed to a smooth variation of the lattice parameter in domain walls of $PbTiO_3$ [24]. The plane adjacent to the domain wall on the tail shows an attractive potential to both charged and neutral oxygen vacancies, indicating an elastic interaction between domain walls and oxygen vacancies. Due to energetically nondegenerate types of oxygen vacancies, the material is likely to exhibit two types of pinning depending on the temperature. The presence of aggregated vacancies at the domain wall may give rise to unique behavior; conduction due to defect-mediated charge hopping is one of the phenomena that is thought to occur at certain domain wall interfaces [35]. Using a combination of temperature, strain, and directional electric field one may pin domain walls in specific locations using oxygen vacancies, thus paving a way for domain-patterned nanodevices. Further calculations on the electronic properties of this wall are necessary to fully understand and take advantage of this phenomena.

ACKNOWLEDGMENTS

A.C., X.W., L.F., and N.S. acknowledge funding received from the European Research Council under the EU 7th Framework Program (FP7/20072013)/ERC Grant Agreement No. 268058, MOBILE-W. We acknowledge that the results of this research have been achieved using the PRACE Research Infrastructure resource FERMI based in Italy at CINECA, Bologna.

[1] J. C. Wojdeł and J. Íñiguez, Phys. Rev. Lett. **112**, 247603 (2014).
[2] T. Sluka, A. K. Tagantsev, D. Damjanovic, M. Gureev, and N. Setter, Nat. Commun. **3**, 748 (2012).
[3] T. Sluka, A. K. Tagantsev, P. Bednyakov, and N. Setter, Nat. Commun. **4**, 1808 (2013).
[4] A. Ohtomo and H. Hwang, Nature (London) **427**, 423 (2004).
[5] G. Herranz, M. Basletić, M. Bibes, C. Carrétéro, E. Tafra, E. Jacquet, K. Bouzehouane, C. Deranlot, A. Hamzić, J.-M. Broto, *et al.*, Phys. Rev. Lett. **98**, 216803 (2007).
[6] J. A. Bert, B. Kalisky, C. Bell, M. Kim, Y. Hikita, H. Y. Hwang, and K. A. Moler, Nat. Phys. **7**, 767 (2011).
[7] J. Seidel, D. Fu, S.-Y. Yang, E. Alarcón-Lladó, J. Wu, R. Ramesh, and J. W. Ager, Phys. Rev. Lett. **107**, 126805 (2011).
[8] S. Liu, F. Zheng, N. Z. Koocher, H. Takenaka, F. Wang, and A. M. Rappe, J. Phys. Chem. Lett. **6**, 693 (2015).
[9] L. Feigl, P. Yudin, I. Stolichnov, T. Sluka, K. Shapovalov, M. Mtebwa, C. S. Sandu, X.-K. Wei, A. K. Tagantsev, and N. Setter, Nat. Commun. **5**, 4677 (2014).
[10] A. Crassous, T. Sluka, A. K. Tagantsev, and N. Setter, Nat. Nanotechnol. **10**, 614 (2015).
[11] L. McGilly, P. Yudin, L. Feigl, A. Tagantsev, and N. Setter, Nat. Nanotechnol. **10**, 145 (2015).
[12] P. Lambeck and G. Jonker, J. Phys. Chem. Solids **47**, 453 (1986).

[13] G. Arlt and H. Neumann, Ferroelectrics **87**, 109 (1988).
[14] U. Robels and G. Arlt, J. Appl. Phys. **73**, 3454 (1993).
[15] L. X. Zhang and X. Ren, Phys. Rev. B **73**, 094121 (2006).
[16] C. H. Park and D. J. Chadi, Phys. Rev. B **57**, R13961 (1998).
[17] J. Scott and M. Dawber, Appl. Phys. Lett. **76**, 3801 (2000).
[18] C. Becher, L. Maurel, U. Aschauer, M. Lilienblum, C. Magén, D. Meier, E. Langenberg, M. Trassin, J. Blasco, I. P. Krug *et al.*, Nat. Nanotechnol. **10**, 661 (2015).
[19] A. Chandrasekaran, D. Damjanovic, N. Setter, and N. Marzari, Phys. Rev. B **88**, 214116 (2013).
[20] Y. Kitanaka, Y. Noguchi, and M. Miyayama, Phys. Rev. B **81**, 094114 (2010).
[21] T. Xu, T. Shimada, Y. Araki, J. Wang, and T. Kitamura, Nano Lett. **16**, 454 (2016).
[22] P. Giannozzi, S. Baroni, N. Bonini, M. Calandra, R. Car, C. Cavazzoni, D. Ceresoli, G. L. Chiarotti, M. Cococcioni, and I. Dabo *et al.*, J. Phys.: Condens. Matter **21**, 395502 (2009).
[23] B. Meyer and D. Vanderbilt, Phys. Rev. B **65**, 104111 (2002).
[24] S. Stemmer, S. K. Streiffer, F. Ernst, and M. Rühle, Philos. Mag. A **71**, 713 (1995).
[25] W. A. Saidi, J. M. P. Martirez, and A. M. Rappe, Nano Lett. **14**, 6711 (2014).
[26] Q. Zhang and W. A. Goddard III, Appl. Phys. Lett. **89**, 182903 (2006).
[27] T. Shimada, T. Ueda, J. Wang, and T. Kitamura, Phys. Rev. B **87**, 174111 (2013).
[28] Z. Alahmed and H. Fu, Phys. Rev. B **76**, 224101 (2007).
[29] Y. Yao and H. Fu, Phys. Rev. B **84**, 064112 (2011).
[30] L. He and D. Vanderbilt, Phys. Rev. B **68**, 134103 (2003).
[31] M. Dawber and J. Scott, Integr. Ferroelectr. **32**, 259 (2001).
[32] P. Paruch, T. Giamarchi, and J.-M. Triscone, Phys. Rev. Lett. **94**, 197601 (2005).
[33] X. Ren, Nat. Mater. **3**, 91 (2004).
[34] M. I. Morozov and D. Damjanovic, J. Appl. Phys. **107**, 034106 (2010).
[35] J. Guyonnet, I. Gaponenko, S. Gariglio, and P. Paruch, Adv. Mater. **23**, 5377 (2011).